Dalton Transactions

ROYAL SOCIETY OF CHEMISTRY

COMMUNICATION

View Article Online
View Journal | View Issue

Cite this: *Dalton Trans.*, 2020, **49**, 13528

Received 15th August 2020,
Accepted 5th September 2020

DOI: 10.1039/d0dt02872j

rsc.li/dalton

Luminescent polypyridyl heteroleptic Cr^{III} complexes with high quantum yields and long excited state lifetimes†

Juan-Ramón Jiménez, *[a] Maxime Poncet,[a] Benjamin Doistau,[a] Céline Besnard[b] and Claude Piguet *[a]

Implementing high quantum yields and long-lived excited state lifetimes within heteroleptic luminescent Cr^{III} complexes is a keystone for the design of supramolecular energy-converting devices exploiting this cheap metal. In this contribution, we discuss the stepwise and rational optimization of these two limiting factors within a series of heteroleptic Cr^{III} complexes.

The on-going interest in emissive polypyridyl-Cr^{III} complexes is well deserved since the Earth's-crust abundance of chromium represents a sustainable and cheaper alternative to the widely used Ru^{II}-based photosensitizers in the field of energy-conversion applications.[1] Compared to the microsecond lifetime and high quantum yield (QY) Metal-to-Ligand Charge-Transfer (MLCT) visible emission characterizing optimized Ru^{II}-polypyridyl complexes,[2,3] Cr^{III} embedded in an analogous pseudo-octahedral strong ligand-field gives rise to long-lived (reaching the millisecond range) intrashell d-d emission bands showing acceptable quantum yields within the NIR domain.[4,5] These bands correspond to the ruby-like metal-centered $Cr(^2E \rightarrow {}^4A_2)$ and $Cr(^2T_1 \rightarrow {}^4A_2)$ spin–flip transitions occurring within the $\pi_{Cr}(t_{2g})$ orbitals. These appealing long excited state lifetimes have made Cr^{III} chromophores attractive sensitizers for maximizing the energy transfer in molecular up-conversion using linear optics[6] and for extending the excited state lifetimes of lanthanide ions *via* downshifting processes.[7] The effective non-radiative mechanisms operating in molecular complexes, in contrast to doped solids, reduce considerably the $Cr(^2E)$ and $Cr(^2T_1)$ lifetimes, and they should be suppressed in order to reach the millisecond range at room temperature. A promising approach uses six-membered chelate rings (*e.g.* ddpd = *N*,*N*′-dimethyl-*N*-*N*′-dipyridine-2-yl-pyridine-2,6 diamine or dqp = 2,6-di(quinolin-8-yl)pyridine, Scheme 1a and b) which (i) reduce structural distortion with respect to a perfect octahedron upon coordination to a single metallic centre and (ii) maximize the metal–ligand orbital overlap, thus inducing considerable ligand field splitting. This strategy was originally proved to be efficient for enhancing both lifetime and QY in Ru^{II} complexes,[2,3] a success further extended to homoleptic Cr^{III} complexes.[4]

The strong ligand field splitting induced by these ligands, together with the near to perfect octahedral geometry of the first coordination sphere (CrN_6), is of crucial importance for restricting non-radiative pathways. In these conditions, back intersystem crossing (BISC) $Cr(^2E/^2T_1 \rightarrow {}^4T_2)$ and potential energy surface crossing between the ground state and the low-lying excited states $(Cr(^2E/^2T_1)–Cr(^4A_2))$ are minimized.[4,9] Moreover, high-energy vibrations (N–H, C–H, O–H) arising from organic ligands or solvents bound to Cr^{III} should be avoided since they represent considerable drawbacks while promoting non-radiative pathways that shorten the lifetime of the spin–flip excited states and reduce the luminescence quantum yields.[9] The classical $[Cr(tpy)_2]^{3+}$ (tpy = 2,2′;6′,2″ terpyridine), $[Cr(phen)_3]^{3+}$ (phen = 1,10-phenanthroline) and $[Cr(bipy)_3]^{3+}$ (bipy = 2,2′-bipyridine) are good examples for the illustration of the aforementioned shortcomings. Firstly, the poor bite angles of the tpy ligand (~79°) reduce the ligand field strength (Scheme 1c), which leads to efficient BISC with

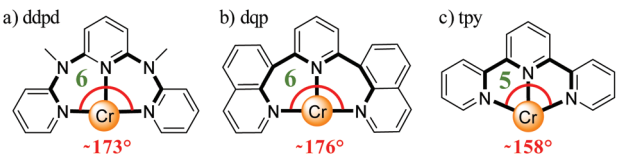

Scheme 1 Binding mode of the tridentate ligands to Cr^{III} considered in this work. (a) (6–6) fused *N*,*N*′-dimethyl-*N*-*N*′-dipyridine-2-yl-pyridine-2,6 diamine chelate, (b) (6–6) fused 2,6-di(quinolin-8-yl)pyridine chelate and (c) (5–5) fused 2,2′;6′,2″ terpyridine chelate.[4,5,8]

[a]*Department of Inorganic and Analytical Chemistry, University of Geneva, 30 quai E. Ansermet, CH-1211 Geneva 4, Switzerland.*
E-mail: Juan.JimenezGallego@unige.ch, Claude.Piguet@unige.ch
[b]*Laboratory of Crystallography, University of Geneva, 24 quai E. Ansermet, CH-1211 Geneva 4, Switzerland*

†Electronic supplementary information (ESI) available. CCDC 2015187–2015190. For ESI and crystallographic data in CIF or other electronic format see DOI: 10.1039/D0DT02872J

the $Cr(^4T_2)$ state.[8,10] Secondly, the strong trigonal distortion provided by phen and bipy ligands promotes additional non-radiative relaxation through surface crossing. In both situations, moderate radiative emission lifetimes and poor QY result.[8] By contrast, the new generation of long and highly emissive pseudo-octahedral homoleptic $[Cr(ddpd)_2]^{3+}$ and $[Cr(dqp)_2]^{3+}$ complexes obtained by the orthogonal binding of two tridentate chelates, each made of two fused six-membered chelate rings, represents nowadays a well-established approach for maximizing both lifetimes and quantum yields. These Cr^{III} complexes have been used in a wide range of applications, such as solar cells,[11] *in vivo* imaging and photodynamic therapy,[12–14] sensing,[15,16] (photo)redox catalysis,[17–20] light-conversion devices,[6,21,22] and circularly polarized light emitters.[5,23] However, the incorporation of these chromophores into optically active supramolecular devices is limited and still underexplored since it requires the preparation of heteroleptic complexes that can act as "building blocks", an issue solved since several decades for Ru(II) chemistry.[24] In this context, the three-step strategy described by Kane-Maguire and co-workers for the synthesis of heteroleptic $[Cr(diimine)_3]^{3+}$,[25] further extended by Constable and co-workers for the synthesis of heteroleptic $[Cr(triimine)_2]^{3+}$,[26] relies on the lability of the $\{Cr–OSO_2CF_3\}$ bond that is easily generated by the reaction of the {Cr–Cl} moieties with trifluoromethanosulfonic acid (CF_3SO_3H). Reaction of the labile intermediate with the additional triimine ligand (L′) generates the corresponding heteroleptic $[(L)Cr(L')]^{3+}$ complex. This method was successfully applied for the construction of luminescent linear $[(tpy)Cr(L)Cr(tpy)]^{6+}$ diads,[27] and for the preparation of versatile heteroleptic Cr^{III} optical sensitizers,[28] and complex-as-ligands,[29] all displaying moderate to low QY and microsecond range $Cr(^2E)$ lifetimes. Seeking longer lifetimes, the luminescent heteroleptic $[Cr(ddpd)(tpy)]^{3+}$ complex and derivatives, which combine a favorable fused (6–6) membered chelate (ddpd) with pernicious terpyridine fused (5–5) membered chelates, showed encouraging long excited-state lifetimes ($\tau(^2E) \sim 1$ ms at 300 K),[30] within the range of those reported for its homoleptic $[Cr(ddpd)_2]^{3+}$ analog.[4] The associated poor QY of *circa* 0.1% was tentatively assigned to the unfavorable structural properties brought by the tpy ligand. However, the preparation of this pioneering heteroleptic (6–6) + (5–5) chelate complexes proved to be not compatible with acidic treatment (CF_3SO_3H) because of the protonation and subsequent decoordination of $[ddpdH]^+$ from the $[Cr(ddpd)Cl_3]$ precursor.[30] Alternatively, the precipitation of Cl^- ions with the help of silver trifluoromethanosulfonate ($AgCF_3SO_3$) affords a highly insoluble AgCl salt and provides the required labile tris-sulfonate $[Cr(ddpd)(OSO_2CF_3)_3]$ complex. The combination of two favourable, but different (6–6)-membered chelates within heteroleptic $[Cr(L)(L')]^{3+}$ complexes has still not been described (to the best of our knowledge) and we report here the pioneering synthesis of a complete series of heteroleptic (6–6) + (5–5) $[Cr(dqp)(tpy)]^{3+}$ (**1**) (6–6) + (6–6) $[Cr(ddpd)(dqp)]^{3+}$ (**2**) and (6–6) + (6–6) $[Cr(dqp)(dqpOMe)]^{3+}$ (**3**) complexes, the structures and photophysical properties of which are described and analyzed.

In line with the Kane–Maguire method,[25] the green $[Cr(dqp)Cl_3]$ precursor was prepared *via* a microwave (MW) assisted reaction between $CrCl_3(THF)_3$ and a stoichiometric amount of the dqp ligand in EtOH at 160 °C. Slow diffusion of diethyl ether into a concentrated DMF solution containing $[Cr(dqp)Cl_3]$ afforded green prismatic crystals suitable for single-crystal X-ray diffraction (Fig. 1).

The neutral complex displays a twisted tridentate dqp ligand meridionally tri-coordinated to the Cr^{III} cation (Cr–N bond lengths = 2.069(4) Å). Three chloride ions complete the coordination sphere (Cr–Cl bond lengths = 2.33(1) Å). The reaction of *mer*-$[Cr(dqp)Cl_3]$ with 3.0 equivalents of $AgCF_3SO_3$ under MW irradiation (30 min, 140 °C) in CH_3CN provided the $[Cr(dqp)(OSO_2CF_3)_3]$ intermediate characterized by ESI-MS (Fig. S1; see the ESI† for the Experimental details). The solution was filtered to remove $AgCl_{(s)}$. Further reaction under MW irradiation with 1.0 equivalent of tpy, ddpd or dqpOMe gave the heteroleptic complexes **1**, **2** and **3** in fair to good yields (Fig. 1). Due to the considerable steric demand of ddpd and dqp ligands, compared to tpy, higher reaction temperatures (120 °C–140 °C) were required to prepare **2** and **3**. However, a temperature of 70 °C was sufficient to prepare **1**, while harsher conditions led to ligand scrambling and mixtures of homo- and heteroleptic complexes. Single crystals of the whole series could be obtained and their structures solved (Tables S1–S12 and Fig. S2–S5†). The Cr–N bond lengths 1.98(1)–2.1(1) Å compare well with those found in related complexes.[4,27,30] In all cases, the second tridentate unit (tpy, ddpd or dqpOMe) coordinates in a meridional way to the $[Cr(dqp)]^{3+}$ unit. In **1**, the tpy ligand is essentially planar while the bound ddpd in **2** or dqpOMe in **3** adopts a twisted arrangement (*P*/*M* helical chirality). As expected, the latter ddpd and dqpOMe ligands

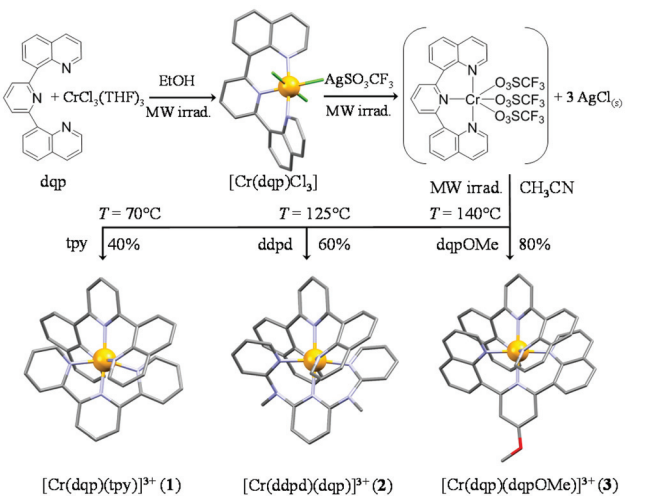

Fig. 1 Synthesis of heteroleptic complexes *via* the $[Cr(dqp)(OSO_2CF_3)_3]$ intermediate. Crystal structures of $[Cr(dqp)Cl_3]$, $[Cr(dqp)(tpy)](PF_6)_3$ (**1**), $[Cr(ddpd)(dqp)](CF_3SO_3)_3$ (**2**) and $[Cr(dqp)(dqpOMe)](CF_3SO_3)_3$ (**3**) are shown. Color code: gray = C, blue = N, red = O and orange = Cr. Hydrogen atoms, counter-anions and solvent molecules have been omitted for clarity.

provide large bite angles of 86–89° ((6–6)-membered chelate rings), which contrast with the shorter bite angles of 76°–79° produced by the tpy ligand ((5–5)-membered chelate rings). Structural distortion with respect to a perfect octahedron can be estimated by using $\sum = \sum_{i=1}^{12} |90 - \phi_i|$, where ϕ_i are the cisoid N–Cr–N bond angles. Thus, **1** shows a less distorted octahedron, Σ = 57°, compared to the previously reported [Cr(ddpd)(tpy)]$^{3+}$ with Σ = 62° due to the minor structural improvement in moving from the ddpd to dqp ligand (the N(terminal)–N(central) distances featured by the bound dqp ligand is 1% longer than in ddpd, Fig. S6†).[30] Similar structural distortion parameters have been calculated for the heteroleptic complexes **2** and **3**, which amount to 30° and 31° respectively, confirming an optimized octahedral geometry as found for the related homoleptic [Cr(ddpd)$_2$]$^{3+}$ complex (Σ = 37°).[4] The twisted (*P* or *M*) and *mer* arrangement adopted for the second ligand (ddpd and dqp) in complexes **2** and **3** is induced by the helical twist found in the racemic starting *mer*-[Cr(*P*-dqp)/(*M*-dqp)Cl$_3$] precursor. Because of (i) steric constraints and (ii) intramolecular interstrand π-stacking occurring between the quinoline rings and the amino-pyridine rings in **2**, or between the two quinoline pairs in **3**,[5] pure racemic *mer-PP*/*MM* mixtures are observed in the crystal structures of **2** and **3** with no trace of either complexes with *fac* configuration or achiral *PM* diastereomers in the crystal (Fig. S7†). Chiral resolution of these racemic mixtures will be explored and reported elsewhere.

Absorption spectra of **1**, **2** and **3** recorded in acetonitrile at room temperature show similar maxima patterns (Fig. 2 and Table S13†). Maxima between 250 and 370 nm are associated with standard π* ← π transitions ($\varepsilon > 10^3$ M^{-1} cm^{-1}). At lower energies, between 370 and 500 nm, the absorption bands are ascribed to a mixture of spin-forbidden ^{3}π* ← π transitions, Ligand-to-Metal Charge-Transfer (LMCT) and Metal Centered (MC) manifold ($\varepsilon < 10^3$ M^{-1} cm^{-1}, Fig. 2a). According to TD-DFT calculations performed for [Cr(ddpd)$_2$]$^{3+}$,[4] and [Cr(dqp)$_2$]$^{3+}$,[5] the shoulder observed in the 400–430 nm range can be assigned to the ligand field spin-allowed Cr(^{4}T$_2$ ← ^{4}A$_2$) transition for compounds **2** and **3**. This transition is observed at lower energies for **1** (472 nm with ε = 634 M^{-1}cm^{-1}, highlighted in Fig. 2a). The pseudo-octahedral ligand field values (Δ) were extracted from the maxima at 472 nm (**1**), 415 nm (**2**) and 409 nm (3). Thus, the Δ value is much lower for [Cr(dqp)(tpy)]$^{3+}$ (**1**, 21 186 cm^{-1}) compared with 24 096 cm^{-1} for [Cr(ddpd)(dqp)]$^{3+}$ (**2**) and 24 449 cm^{-1} for [Cr(dqp)(dqpOMe)]$^{3+}$ (**3**). These values are in line with the strong ligand-field parameters found in the homoleptic model (6–6)-membered chelate [Cr(ddpd)$_2$]$^{3+}$ (Δ = 23 000 cm^{-1}) and [Cr(dqp)$_2$]$^{3+}$ (Δ = 24 937 cm^{-1}) complexes and the (6–6) + (5–5) membered heteroleptic complex [Cr(ddpd)(tpy)]$^{3+}$ (Δ = 20 121 cm^{-1}).[30] The latter suffers from a smaller ligand field splitting because of the poor bite angle provided by the tpy ligand. At lower energies (670–800 nm), the weak spin–flip Cr(^{2}E ← ^{4}A$_2$) and Cr(^{2}T$_1$ ← ^{4}A$_2$) transitions (ε = 0.1–1 M^{-1}cm^{-1}) could be evidenced (Fig. 2b and Table S13†). The symmetry release in moving from *O* to C_2 for **1–3** lifts any orbital degeneracy,

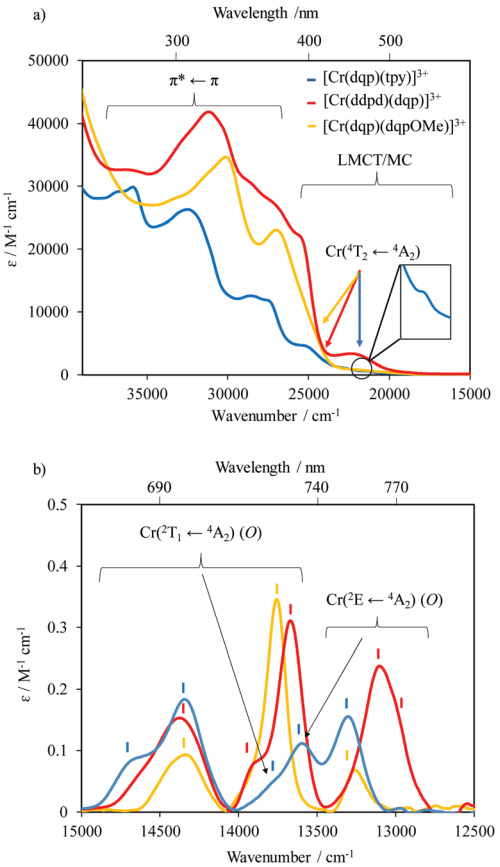

Fig. 2 Absorption spectra of **1** (blue trace), **2** (red trace) and **3** (orange trace) recorded in (a) acetonitrile solution (2 × 10^{-4} M) between 250 and 500 nm; the orange, red and blue arrows point to the Cr(^{4}T$_2$ ← ^{4}A$_2$) transition for each complex and (b) acetonitrile solution (5 × 10^{-3} M) between 650 and 800 nm at 293 K. The vertical dashes in (b) represent the different transitions due to the lowering in symmetry in moving from *O* to C_2 (see text).

leading to a maximum of (i) three transitions on the high energy side gathered under the octahedral symbol Cr(^{2}T$_1$ ← ^{4}A$_2$) and (ii) two transitions for Cr(^{2}E ← ^{4}A$_2$) at lower energies as observed for [Cr(dqp)(tpy)]$^{3+}$ and [Cr(ddpd)(dqp)]$^{3+}$. For [Cr(dqp)(dqpOMe)]$^{3+}$ (**3**), the two bound ligands are so similar that the splitting is reduced to such an extent that two bands are indeed observed for Cr(^{2}E ← ^{4}A$_2$), but only one broad unsymmetrical band is detected for Cr(^{2}T$_1$ ← ^{4}A$_2$) (Fig. 2b, yellow trace).

Upon excitation at 435 nm at room temperature, the complexes exhibit two sharp emission bands (full width at half height, FWHH ≈ 250 cm^{-1}) with maxima at 746 nm (13 404 cm^{-1}) and 724 nm (13 812 cm^{-1}) for **1**, 762 (13 123 cm^{-1}) and 728 nm (13 736 cm^{-1}) for **2** and 752 nm (13 297 cm^{-1}) and 725 nm (13 793 cm^{-1}) for **3** (Fig. 3a). Full emission spectra from 550 to 850 nm for complexes **2** and **3** did not show any residual fluorescence in this range (Fig. S10†) and their excitation spectra closely match the absorption spectra (Fig. S11†). The low energy and high energy bands correspond to the spin–flip Cr(^{2}E → ^{4}A$_2$) and

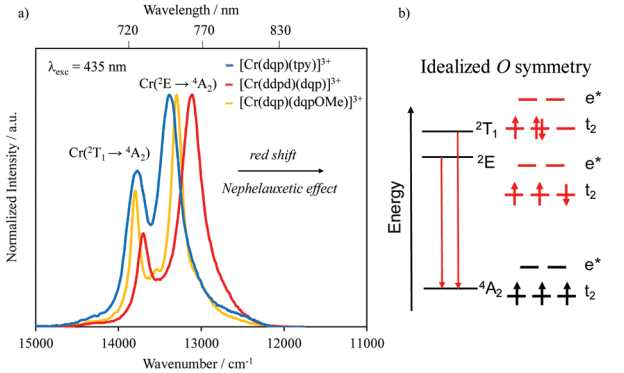

Fig. 3 (a) Emission spectra of **1** (blue trace), **2** (red trace) and **3** (orange trace) recorded in deaerated acetonitrile solution (10^{-4} M) between 650 and 850 nm at room temperature (λ_{exc} = 435 nm). (b) Schematic representation of the Cr^{III} spin–flip transitions according to an idealized octahedral strong-ligand field splitting.

Cr(^{2}T$_1$ → ^{4}A$_2$) transitions, respectively (Fig. 3b). The Racah interelectronic repulsion parameters (B and C) could be extracted with the help of eqn (S1)–(S3) (see the ESI†).[31,32] The computed parameters show a slight increase of the nephelauxetic effect as follows: **2** > **3** > **1** which explains the total 254 cm^{-1} red shift in moving from **1** to **2** (Table S14†). The room temperature overall quantum yields amount to 0.2(1)%, 6.0(5)% and 6.5(5)%, respectively, for **1**, **2** and **3**, with $\tau^{^2T_1} = \tau^{^2E}$ ranging from 578 to 855 μs in deaerated solutions (Table 1 and Fig. S8†). The satisfying 578 μs lifetime, but the associated low quantum yield (0.2%), observed for $[Cr(dqp)(tpy)]^{3+}$ (**1**) mirror those reported for analogous $[Cr(ddpd)(tpy)]^{3+}$ (1.0 ms and QY = 0.06% in deaerated acetonitrile).[30] This confirms the deleterious effect of the tpy ligand on the photophysical properties in heteroleptic Cr^{III} complexes, although the latter remains much more favourable than those found in the archetypal $[Cr(tpy)_2]^{3+}$ (τ < 1 μs and QY < 0.0001%).[8,33] The long excited-state lifetimes together with high QY displayed by **2** and **3** confirm the optimization of the photophysical properties in heteroleptic $[CrN_6]$ chromophores containing only fused (6–6) membered chelate rings. Moreover, these values are among the highest reported so far for deuterium-free Cr^{III} complexes in organic solutions.[11,34] In aerated acetonitrile solutions, those values are reduced by orders of magnitude due to quenching by $^3O_2$ (Table S15†).

At 77 K, in frozen acetonitrile solutions, the excited state lifetimes are considerably extended for **2** and **3** (1.7 ms and 2.7 ms, respectively) which evidences the removal of efficient thermally activated non-radiative processes (Fig. S8, S9 and Table S15†). For **1**, $\tau_{77\,K}$ remains in the same order of magnitude as at room temperature, indicating the operation of non-radiative deactivation pathways with minor energy barriers (Table S15†). Finally, the spin–flip transitions' radiative rate constants k_{rad} < 100 s^{-1} were extracted from the absorption spectra (Table S15†) together with the intrinsic quantum yields $\Phi_{Cr}^{Cr} = k_{rad}\tau_{obs}$ (0.9% ≤ Φ_{Cr}^{Cr} ≤ 4% for emission from Cr(^{2}E), 3.4% ≤ Φ_{Cr}^{Cr} ≤ 5.8% for emission from Cr(^{2}T$_1$) in deaerated acetonitrile) and energy transfer efficiency $\eta_{sens}^{L\rightarrow Cr} = \Phi_{Cr}^{L}/\Phi_{Cr}^{Cr}$ for funnelling the energy from the ligand excited states onto the emissive Cr^{III} excited levels. The latter parameter appears to be crucial in controlling the global QY because $\eta_{sens}^{L\rightarrow Cr}$ increases from 3.0(5)% for $[Cr(dqp)(tpy)]^{3+}$ (**1**) to 61(5)% for $[Cr(ddpd)(dqp)]^{3+}$ (**2**) and 100(7)% for $[Cr(dqp)(dqpOMe)]^{3+}$ (**3**) (Table S15†).

In conclusion, the replacement of Cl^- with $CF_3SO_3^-$ *via* a microwave-assisted reaction appears to be a reliable and general strategy for the generation of labile $[(L)Cr(OSO_2CF_3)_3]$ starting materials for the preparation of the target heteroleptic Cr^{III} complexes. Applying this method results in the isolation of the first heteroleptic Cr^{III} complexes with two different tridentate fused (6–6)-membered chelate rings. The favourable structural and electronic properties of the latter systems lead to long excited state lifetimes (>600 μs) and high quantum yields (>5%), which make these chromium complexes a sustainable alternative to expensive precious metal-based complexes, for their insertion into heterometallic supramolecular architectures within the frame of energy-conversion technologies.

Table 1 Cr(^{2}E) and Cr(^{2}T$_1$) excited-state lifetimes and overall quantum yields determined for $[Cr(dqp)(tpy)]^{3+}$ (**1**), $[Cr(ddpd)(dqp)]^{3+}$ (**2**), $[Cr(dqp)(dqpOMe)]^{3+}$ (**3**), $[Cr(ddpd)_2]^{3+}$(ref. 4) and $[Cr(dqp)_2]^{3+}$ (ref. 3) in solution

Compounds	$\tau_{293\,K}$ [a]/μs	Φ_{Cr}^{L} [a,b]/%
$[Cr(dqp)(tpy)]^{3+}$	578(10)	0.2(1)
$[Cr(ddpd)(dqp)]^{3+}$	642(10)	6.0(5)
$[Cr(dqp)(dqpOMe)]^{3+}$	855(10)	6.5(5)
$[Cr(ddpd)_2]^{3+}$	886	12.1
$[Cr(dqp)_2]^{3+}$ [c]	1200(20)	7.3(4)

[a] Measurement in deaerated acetonitrile solution (≈10^{-5} M) at room temperature. [b] Overall QY calculated obtained with a comparative method using $[Cr(ddpd)_2]^{3+}$ as reference (Φ_{Cr}^{L} = 12.1%; λ_{exc} = 435 nm). [c] In deaerated water.

Conflicts of interest

There are no conflicts to declare.

Notes and references

1 O. S. Wenger, *J. Am. Chem. Soc.*, 2018, **140**, 13522–13533.
2 M. Abrahamsson, M. Jäger, T. Österman, L. Eriksson, P. Persson, H. C. Becker, O. Johansson and L. Hammarström, *J. Am. Chem. Soc.*, 2006, **128**, 12616–12617.
3 M. Abrahamsson, H. C. Becker and L. Hammarström, *Dalton Trans.*, 2017, **46**, 13314–13321.
4 S. Otto, M. Grabolle, C. Förster, C. Kreitner, U. Resch-Genger and K. Heinze, *Angew. Chem., Int. Ed.*, 2015, **54**, 11572–11576.

5 J.-R. Jiménez, B. Doistau, C. M. Cruz, C. Besnard, J. M. Cuerva, A. G. Campaña and C. Piguet, *J. Am. Chem. Soc.*, 2019, **141**, 13244–13252.
6 L. Aboshyan-Sorgho, C. Besnard, P. Pattison, K. R. Kittilstved, A. Aebischer, J.-C. G. Bünzli, A. Hauser and C. Piguet, *Angew. Chem., Int. Ed.*, 2011, **50**, 4108–4112.
7 D. Imbert, M. Cantuel, J. C. G. Bünzli, G. Bernardinelli and C. Piguet, *J. Am. Chem. Soc.*, 2003, **125**, 15698–15699.
8 N. Serpone, M. A. Jamieson, M. S. Henry, M. Z. Hoffman, F. Bolletta and M. Maestri, *J. Am. Chem. Soc.*, 1979, **101**, 2907–2916.
9 S. Otto, M. Dorn, C. Förster, M. Bauer, M. Seitz and K. Heinze, *Coord. Chem. Rev.*, 2018, **359**, 102–111.
10 J. R. Jiménez, B. Doistau, C. Besnard and C. Piguet, *Chem. Commun.*, 2018, **54**, 13228–13231.
11 L. A. Büldt and O. S. Wenger, *Chem. Sci.*, 2017, **8**, 7359–7367.
12 Z. Zhou, M. Yu, H. Yang, K. Huang, F. Li, T. Yi and C. Huang, *Chem. Commun.*, 2008, 3387–3389.
13 J. Toneatto, P. F. Garcia and G. A. Argüello, *J. Inorg. Biochem.*, 2011, **105**, 1299–1305.
14 U. Basu, S. Otto, K. Heinze and G. Gasser, *Eur. J. Inorg. Chem.*, 2019, 37–41.
15 S. Otto, J. P. Harris, K. Heinze and C. Reber, *Angew. Chem., Int. Ed.*, 2018, **57**, 1–6.
16 S. Otto, N. Scholz, T. Behnke, U. Resch-Genger and K. Heinze, *Chem. – Eur. J.*, 2017, **23**, 12131–12135.
17 A. M. McDaniel, H. W. Tseng, N. H. Damrauer and M. P. Shores, *Inorg. Chem.*, 2010, **49**, 7981–7991.
18 S. M. Stevenson, M. P. Shores and E. M. Ferreira, *Angew. Chem., Int. Ed.*, 2015, **54**, 6506–6510.
19 S. Otto, A. M. Nauth, E. Ermilov, N. Scholz, A. Friedrich, U. Resch-Genger, S. Lochbrunner, T. Opatz and K. Heinze, *ChemPhotoChem*, 2017, **1**, 344–349.
20 B. E. Olafsen, G. V. Crescenzo, L. P. Moisey, B. O. Patrick and K. M. Smith, *Inorg. Chem.*, 2018, **57**, 9611–9621.
21 M. Cantuel, G. Bernardinelli, D. Imbert, J.-C. G. Bünzli, G. Hopfgartner and C. Piguet, *J. Chem. Soc., Dalton Trans.*, 2002, 1929–1940.
22 L. Aboshyan-Sorgho, H. Nozary, A. Aebischer, J. C. G. Bünzli, P. Y. Morgantini, K. R. Kittilstved, A. Hauser, S. V. Eliseeva, S. Petoud and C. Piguet, *J. Am. Chem. Soc.*, 2012, **134**, 12675–12684.
23 C. Dee, F. Zinna, W. R. Kitzmann, K. Heinze, D. Bari and M. Seitz, *Chem. Commun.*, 2019, **55**, 13078–13081.
24 T. Mede, M. Ja, U. S. Schubert and T. Mede, *Chem. Soc. Rev.*, 2018, **47**, 7577–7627.
25 K. D. Barker, K. A. Barnett, S. M. Connell, J. W. Glaeser, A. J. Wallace, J. Wildsmith, B. J. Herbert, J. F. Wheeler and N. A. P. Kane-Maguire, *Inorg. Chim. Acta*, 2001, **316**, 41–49.
26 J. Schönle, E. C. Constable, C. E. Housecroft, A. Prescimone and J. A. Zampese, *Polyhedron*, 2015, **89**, 182–188.
27 D. Zare, B. Doistau, H. Nozary, C. Besnard, L. Guénée, Y. Suffren, A.-L. Pelé, A. Hauser and C. Piguet, *Dalton Trans.*, 2017, **46**, 8992–9009.
28 B. Doistau, G. Collet, E. A. Bolomey, V. Sadat-Noorbakhsh, C. Besnard and C. Piguet, *Inorg. Chem.*, 2018, **57**, 14362–14373.
29 B. Doistau, J.-R. Jiménez, S. Guerra, C. Besnard and C. Piguet, *Inorg. Chem.*, 2020, **59**, 1424–1435.
30 J.-R. Jiménez, B. Doistau, C. Besnard and C. Piguet, *Chem. Commun.*, 2018, **54**, 13228–13231.
31 C. K. Jorgensen, *Adv. Chem. Phys.*, 1963, **5**, 33–146.
32 A. B. P. Lever, in *Inorg. Electron. Spectrosc*, Elsevier, Amsterdam, Oxford, New York, Tokyo, 2nd edn, 1984, pp. 126.
33 J. C. Barbour, A. J. I. Kim, E. DeVries, S. E. Shaner and B. M. Lovaasen, *Inorg. Chem.*, 2017, **56**, 8212–8222.
34 C. Wang, S. Otto, M. Dorn, E. Kreidt, J. Lebon, L. Sršan, P. DiMartino-Fumo, M. Gerhards, U. Resch-Genger, M. Seitz and K. Heinze, *Angew. Chem., Int. Ed.*, 2018, **57**, 1112–1116.